Effects of 3D Thermal Radiation on Cloud Development

Carolin Klinger[1], Bernhard Mayer[1], Fabian Jakub[1], Tobias Zinner[1], Seungbu Park[2], and Pierre Gentine[2]

[1]Ludwig Maximilians-Universität München, Fakultät für Physik, Meteorologisches Institut München
[2]Department of Earth and Environmental Engineering, Earth Institute, Columbia University, New York, New York

Correspondence to: Carolin Klinger (carolin.klinger@physik.lmu.de)

Abstract. We investigate the effects of thermal radiation on cloud development in an idealized setup in large-eddy simulations with the UCLA-LES model. We investigate single convective clouds (driven by a warm bubble) and a large cumulus cloud field at 50 m horizontal resolution. We compare the newly developed 3D "neighboring column approximation" with the independent column approximation and a simulation without radiation and their respective impact on clouds. Thermal radiation causes

5   strong local cooling at cloud tops accompanied by a modest warming at the cloud bottom, and in the case of a 3D scheme, also cloud side cooling. 3D thermal radiation causes systematically larger cooling when averaged over the model domain. In order to investigate the effects of local cooling on the clouds and to separate these local effects from a systematically larger cooling effect in the modeling domain, we apply the radiative transfer solutions in different ways. The direct effect of heating and cooling at the clouds is applied (interactive thermal radiation) in a first simulation. Furthermore, a slab-averaged applica-

10   tions of the 1D and 3D radiation is used to study the effect of local cloud radiation as opposed to the domain averaged effect. These simulations exhibit a cooling profile, with stronger cooling in the cloudy layers. In a final setup, we replace the radiation simulation by a uniform cooling of 2.6 K/d.

For the simulations of isolated single cloud, or the cumulus cloud field with interactive radiation, we find that thermal radiation changes cloud circulation, by causing stronger updrafts and stronger subsiding shells.

15   In our cumulus cloud field simulation we find that interactive radiation, acting locally on clouds, enhances the circulation compared to the averaged radiation applications. In addition we find that thermal radiation triggers the organization of clouds. Comparing the effects of 3D and 1D thermal radiation, we find that organization effects of 3D thermal radiation are usually stronger than the 1D counterpart (either interactive or averaged). Interactive radiation leads to an earlier onset of the organization both in 1D and 3D compared to the averaged radiation application. Applying a constant cooling to the simulations leads to

20   a similar development of the cloud field as in the case of averaged radiation, but less water condenses overall in the simulation. Generally, clouds contain more liquid water if radiation is accounted for. Furthermore, thermal radiation enhances turbulence and mixing as well as the size and lifetime of clouds. Interactive thermal radiation produces larger clouds with longer lifetimes.

1   Introduction

25   Clouds are a the key element for accurate climate and weather prediction and cause large uncertainties in the prediction of both (Boucher et al., 2013). Clouds play an important, yet poorly quantified role in climate change. Key questions arising from the

limited understanding of clouds in climate prediction were recently pointed out by Bony et al. (2015). These questions include the role of cloud organization or the role of cloud convection in a changing climate.

Solar and thermal radiation drive weather and climate and affect cloud formation. Former studies using accurate radiative transfer models (e.g. Monte Carlo Models) found strong local thermal cooling rates reaching up to 300-600 K/d (e.g. Kablick et al. (2011); Klinger and Mayer (2014)) in realistic cloud field simulations. It was shown that 3D cooling rates exceed 1D cooling rates both in magnitude and by an additional cloud side cooling. An example of 3D thermal cooling rates in a cumulus cloud field (calculated on an LES time snapshot from Cahalan et al. (2005)) is shown in Fig. 1. The figure shows cooling rates at cloud tops and cloud sides, reaching values up to 300 K/d. In addition, modest warming at the cloud bottom (maximum 30 K/d) is found. The difference in the surface flux between cloud free and cloudy areas is small in the thermal spectral range. The magnitude of these cooling rates suggests that thermal radiation likely has an impact on cloud development. Indeed, thermal radiation can modify the development of clouds in two different ways: by changing the dynamics and microphysics. Former studies assessing the effect of thermal radiation on dynamics mainly used 1D radiative transfer codes. Studies with 3D radiative transfer are rare. Guan et al. (1995, 1997) showed that thermal radiation increases the liquid water content of clouds and causes an additional downward motion at the interface between the cloud and the atmosphere. They used a 3D radiative transfer approximation, which, however was limited to axially symmetric clouds. The change in cloud circulation in turn promoted vertical cloud development. The vertical differential local heating and cooling causes a destabilization of the cloud (Fu et al., 1995), which increases buoyancy (Sommerai, 1976) and also turbulence production in clouds (Davies and Alves, 1989; Fu et al., 1995; Petters et al., 2012). Fu et al. (1995) also found that the clear sky cooling enhances convection and precipitation. Larson et al. (2001) showed that thermal cooling on the one hand enhances condensation and thus increases liquid water content; on the other hand, radiation causes more entrainment and therefore a decrease in liquid water content. Xu and Randall (1995) found a longer lifetime of clouds when simulating clouds with interactive radiation. They compared simulations with interactive radiation to a homogenized application to look at the local effects of differential heating and cooling on deep convective clouds. Thermal radiation increased turbulence on short time scales, and on longer time scales the cloud development itself. A similar approach was followed by Xiao et al. (2014). In this case, simulations with interactive and homogenized radiation where performed, with a focus on stratocumulus to cumulus transition. Again, an increase in turbulence, due to the destabilization of the clouds by thermal radiation was found. Xiao et al. (2014) state that because they only used a common 1D approximation for the radiation calculation the effects might be larger with 3D radiation. The hypothesis of destabilization of the cloud layer by thermal radiation was originally proposed by Lilly (1988). Tao et al. (1993) found an increase in precipitation of 14-31% due to thermal effects and Tao et al. (1996) saw an increase in relative humidity, enhanced circulation and microphysical processes. In a recent study, Bellon and Geoffroy (2016a) investigated the stratocumulus radiative effect in a set of equilibrium simulations. It was found that depending on the sea surface temperature, radiative cooling at cloud top is either crucial for the existence of the stratocumulus clouds or causes enhanced turbulence by buoyancy production, more entrainment and a deepening of the boundary layer. Based on the results of the first study (Bellon and Geoffroy, 2016a), Bellon and Geoffroy (2016b) investigated how good the stratocumulus radiative effect has to be represented. Applying different radiative solutions, such as column or horizontally averaged radiation, Bellon and Geoffroy (2016b) found that the radiative effect has to

be represented in some detail at the cloud top to account for the enhanced turbulence and mixing and therefore determining the existence of the stratocumulus. Studies by Muller and Held (2012); Muller and Bony (2015) suggest that interactive thermal radiation is essential to trigger self-organization in radiative-convective-equilibrium simulations. Emanuel et al. (2014) found that clear sky thermal cooling is also a key component for self-organization.

5   The microphysical aspect was further addressed e.g. by Harrington et al. (2000); Marquis and Harrington (2005). They showed that thermal emission enhances cloud droplet growth by diffusion. An earlier onset of collision and coalescence of cloud droplets was found by Hartman and Harrington (2005a) and Hartman and Harrington (2005b) when thermal radiation is considered. Recent studies of Brewster (2015) and de Lozar and Muessle (2016) emphasize the hypothesis that thermal radiation might influence droplet growth significantly and lead to a broadening of the droplet size spectra and thus enhance the formation

10 of precipitation.

These former studies were mostly based on 1D radiative transfer approximation. Studies accounting for 3D effects are rare. This paper aims to address the interaction of radiation and clouds, including a comparison of the effects of 1D and 3D thermal radiation. For this 3D interactive radiation (the "Neighboring Column Approximation", NCA; Klinger and Mayer (2016)) was incorporated into the UCLA-LES (Stevens et al., 2005; Stevens, 2007) and a set of idealized simulations was developed, aiming

15 to isolate the effect of 1D and 3D thermal radiation on clouds. The model and model setup are described in Section 2. The results are presented in Section 3.

2   Simulation Setup

The University of California Los Angeles Large Eddy Simulation model (UCLA-LES; Stevens et al. (2005); Stevens (2007)) is

20 used for our analysis. The model has previously been successfully used to represent various typical cases, including BOMEX (Cheng et al., 2010), RICO (van Zanten et al., 2011) or DYCOMS (Stevens et al., 2005). The standard UCLA-LES includes bulk microphysics for warm clouds (Seifert and Beheng, 2001) and a 1D radiation scheme (δ-four-stream, Liou et al. (1988)). The spectral integration is accounted for with a correlated-k molecular absorption parameterization (Fu and Liou, 1992). In addition the Monte Carlo spectral integration (MCSI; Pincus and Stevens (2009)) is used in this study for the simulation of

25 the cumulus cloud field to save computational time. The UCLA-LES was adapted for 3D interactive thermal radiation by implementing the "Neighboring Column Approximation", (NCA; Klinger and Mayer (2016)) for the calculation of 3D thermal heating and cooling rates.

Two passive scalar tracers were implemented into UCLA-LES, following Park et al. (2016). With the help of the tracers, we performed an octant analysis (Park et al., 2016) to extract coherent structures in simulation data. For further analysis of the

30 results, we used the cloud tracking algorithm Cb-TRAM (Zinner et al., 2008).

2.1 UCLA-LES Setup

Two different types of idealized cloud studies have been performed, with either a single cloud or a complete cumulus cloud field.

Single Cloud

A single cloud, induced by a heat bubble is investigated to study the effects of thermal radiation on individual clouds. We compare the effects of a simulation without radiation (*No-Radiation*) to simulations with 1D independent column approximation interactive (*1D Thermal ICA*) and simulations with 3D thermal radiation (*3D Thermal NCA*) using the NCA. For the simulation, the full thermal spectrum was simulated.

As the strength of the radiation effect on cloud development likely depends on the shape and dynamics of a cloud, we choose four different clouds for our investigation.

– A weakly driven, axially symmetric cloud. The heat bubble is introduced by a elliptical shaped volume of warmer air close to the surface. The temperature perturbation is 0.4 K.

– A weakly driven, non-symmetric cloud. The heat bubble is introduced by a uniform random perturbation varying between 0.0 - 0.8 K in the same elliptical shaped volume as the weakly driven symmetric cloud, giving the same average perturbation of 0.4 K as above. The cloud is comparable in strength to the weakly driven axially symmetric cloud.

– A stronger driven, axially symmetric cloud. The heat bubble is introduced by a elliptical shaped volume of warmer air close to the surface. The temperature perturbation is 0.8 K.

– A stronger driven, non-symmetric cloud. The heat bubble is introduced by a uniform random perturbation varying between 0.0 - 1.6 K in the same elliptical shaped volume as the stronger driven symmetric cloud, giving the same average perturbation of 0.8 K as above. The cloud is comparable in strength to the stronger driven axially symmetric cloud.

A stable background profile was chosen in order to cause only moderate updraft velocities of a few m/s. The simulation is performed over 80 min. More setup details are summarized in Tab. 1. The random noise in the non-symmetric cloud simulations was initialized with the same random seed in all simulations in order to simulate clouds of similar shape which allows a direct comparison of the development of the clouds. The simulations are performed with 50 m horizontal and vertical resolution in a 6.4 x 6.4 km^2 domain.

Cumulus Cloud Field

Large scale simulations of a cumulus cloud field in a 50x50 km^2 domain with 50 m horizontal resolution have been performed. The environment was a warm ocean surface without orography. All simulations are run for 30 hours at Deutsches Klima Rechenzentrum (DKRZ) in Hamburg on Mistral supercomputer (Intel-Haswell) on 512 cores. We focused on the effects of thermal radiative heating and cooling at the clouds itself. Therefore, surface fluxes of latent (180 W/m^2) and sensible heat (18 W/m^2) were fixed throughout the simulation. The initial atmospheric profiles for this simulations were taken from Stevens

(2007). We allow for warm microphysics (Seifert and Beheng, 2001), but omit the development of rain to reduce possible feedbacks that rain might cause (e.g. cold pool dynamics). Due to the high computational costs of radiation simulations, we used the Monte Carlo Spectral Integration (MCSI, Pincus and Stevens (2009)) in a version adapted for 3D interactive radiation described in Jakub and Mayer (2015). Further details are given in Tab. 2.

5 Again, we compare different radiation types (*1D Thermal ICA* and *3D Thermal NCA*). Those are the *interactive radiation* applications, where heating and cooling acts locally where it is generated. In addition, we *averaged* the thermal heating and cooling of the *1D Thermal ICA* and *3D Thermal NCA* radiation solution in each time step in each layer (*1D Thermal AVG* and *3D Thermal AVG*). This allows us to separate the effects of local heating/cooling in comparison to a systematically higher cooling that is introduced by thermal radiation. In addition we can separate possible feedbacks that might arise from the

10 different amount of cooling introduced by the 1D and 3D radiative transfer solutions. The overall cooling in a modeling domain is generally stronger in case of *3D thermal NCA* radiation. Additionally, we apply a *constant cooling* of 2.6 K/d throughout the simulation in the modeling domain. The constant cooling differs from the *averaged radiation* simulations in the profile of the cooling. The *averaged radiation* simulations cause more cooling in the cloudy layers.

All simulations are analyzed after a 3h initialization run, where the first clouds are allowed to form.

15 2.2 Cb-TRAM Cloud Tracking Algorithm

To gain some statistics on the cloud size, lifetime and number of clouds in the simulations, we use a cloud tracking algorithm to track individual clouds over time. Cb-TRAM was originally setup to work with satellite imagery by (Zinner et al., 2008), but is easily adapted to any other map of 2D information. Here fields of liquid water path are tracked. Cb-TRAM identifies objects as contiguous areas with a specific common characteristic. We set two thresholds to define a cloud: first, only cloud columns

20 of a liquid water path larger then 20 g/m^2 are considered; second, a cloud must consist at least of 16 grid connected boxes. Objects defined this way at one time step are found in the water path field of the next time step using an optical flow analysis of the liquid water field deformation and a simple object overlap analysis. This way cloud objects are detected and tracked over time, allowing us to estimate cloud size and lifetime distributions.

3 Simulations Results

25 3.1 Single Cloud Simulations

Figure 2 provides a first impression of the four different single cloud simulation. The visualization shows the weak symmetric, weak non-symmetric, strong symmetric and strong non-symmetric single cloud simulations at 20 min for the *No-Radiation* simulation. The following section provides a detailed analysis of the development of these single clouds for different radiation setups.

30 A comparison of the time development of liquid water, vertical velocity and cooling rates is shown in Fig. 3 and Fig. 4. Liquid water path is sampled for the original cloud only (*conditionally sampled*). During the simulations, new clouds form close to

the surface, which we ignore in our analysis. Also, cooling rates are sampled and averaged over grid boxes belonging to this single cloud, to show heating and cooling generated by the cloud. A running average over 300 s was applied to the averages in order to smooth the results. A gray shaded area covers the first 40 min of the simulations in Fig. 3 and Fig. 4. During this time, the cloud development is dominated by the heat perturbation of the warm bubble. Updraft vertical velocities are strong in this

5   initial stage. We only expect an significant effect of thermal radiation on cloud development after that initial stage. Interestingly, 40 min is about the time it takes for the thermal cooling to compensate the original heat perturbation of the bubble (not shown).

Both, the symmetric and non-symmetric clouds show the impact of thermal radiation on the cloud development. Focusing on the liquid water path (top row of Fig. 3) we can split the cloud development into three stages. Both cloud types show a fast

10   development at the beginning (up to about 20 min, gray shaded area, until first gray line). We refer to this first development of the cloud as the "first stage". During that time, the development is dominated by the heat perturbation at the surface. Both liquid water quantities develop similarly in all simulations, with only little differences due to thermal radiation.

After the first stage, liquid water path decreases and finally, from about 30 min onward the cloud stays rather constant at a certain height (not shown). Updrafts become weaker (top row of Fig. 4) and radiation acts more significantly on the cloud.

15   All simulations show that the liquid water path (top row of Fig. 3) is reduced by thermal radiation in this "second stage" (from about 20 min to 40 min). The "last stage" of cloud development (about 40 min to 80 min) is dominated by a second growth-period of the cloud. In this stage, thermal radiation can act on the cloud. From this time on, the initial heat perturbation is compensated by thermal cooling. Both non-symmetric clouds show a second rise in liquid water path, in case of the stronger forced cloud exceeding the *No-Radiation* simulation. Interestingly, when comparing the development of liquid water path to

20   the development of maximum liquid water mixing ratio over time (lower row of Fig. 3) the rise in liquid water mixing ratio in the last phase becomes more evident. Maximum values of liquid water mixing ratio in the radiation simulations exceed the *No-Radiation* simulation in this last phase. Looking at the location of these maximum values of liquid water mixing ratio and the shape of the cloud (not shown), we find that clouds become narrower (have a reduced horizontal extent) over time when radiative effects are accounted for and maxima of liquid water mixing ratio are enhanced in the center of the cloud. Vertical

25   velocities show stronger upward and downward values for both thermal radiation simulations. The upward and downward motion at this time results from the initial temperature perturbation and the resulting overturning circulation.

Looking at the differences between *1D Thermal ICA* and *3D Thermal NCA* we find stronger cooling in the *3D Thermal NCA* radiation simulation which affect the further development of the cloud (bottom row of Fig. 4). Differences occur in terms of liquid water when comparing both thermal radiation simulations. The differences are small though, but in general slightly

30   stronger in the case of *3D Thermal NCA* simulation. In the last stage, differences in vertical velocity between the *No-Radiation* and the *thermal radiation* simulations are evident. Both radiation simulations show stronger upward and downward vertical velocities. Vertical velocities are usually a bit stronger in case of *3D Thermal NCA* radiation than in case of 1D thermal radiation. Combining the development of liquid water with upward and downward vertical velocities (top and middle row of Fig. 4), the data suggests that a change in cloud circulation is induced from the second stage onward by the effects of thermal radiation,

35   which enhances updraft vertical velocities in the cloud cores, thus strengthening the cloud development and at the same time,

induces stronger downdraft vertical velocities at the cloud sides.

The region of subsiding motion around a cloud, the "subsiding shell" is known from previous work of Heus and Jonker (2008); Jiang et al. (2006); Small et al. (2009). Heus and Jonker (2008) studied the subsiding shell of cumulus clouds from measurement data in comparison to model simulations and concluded that negative buoyancy at the cloud sides causes the subsiding

5 shell to develop. Jiang et al. (2006) and Small et al. (2009) again compared measurement data and simulations. They found a stronger subsiding shell due to more cloud condensation nuclei and enhanced evaporative cooling in their study. Stronger downward motion at cloud sides was also found by Guan et al. (1995) and Guan et al. (1997) due to the effect of thermal radiation.

We found that thermal radiation has an effect on the cloud development from the end of the second stage on, when the cloud

10 stays at a constant height and the initial temperature perturbation is compensated by thermal cooling. To further investigate this question and the development of the cloud, with a special focus on the possible change in cloud circulation and the subsiding shell, Fig. 5 shows transects of liquid water (bottom of each figure) and vertical velocity (center of each figure) in the last stage of cloud development, averaged in 900-1200 m height (in the cloud layer).

In the time series analysis, the cloud development is accompanied by stronger updrafts and stronger downdrafts in the radiation

15 simulations. Fig. 5 shows the stronger upward and downward motion in the transect. The subsiding shells are clearly visible at the cloud side region. Liquid water content is enhanced in the radiation simulations in the cloud center and the cloud is narrower (Fig. 5). This is in agreement with the results of the time development of liquid water path and maximum liquid water (Fig. 3) that indicated narrower clouds with enhanced liquid water content in the cloud center. Stronger downdrafts are found for all radiation simulations. Again, clouds simulated with the radiative feedback are narrower.

20 Finally, Fig. 6 shows the horizontally averaged vertical profile of negative and positive buoyancy, sampled in the cloudy region (all grid boxes where liquid water is larger than zero). Data is sampled for 8 min, starting after 50 min of the simulation. All simulations including thermal radiation show stronger negative buoyancy which is slightly larger in the *3D Thermal NCA* is slightly larger than in the 1D case. This might be due to the thermal cooling at cloud tops, and in case of *3D Thermal NCA* radiation at cloud sides. The negative buoyancy can cause the observed subsiding motion, as already found by Heus and Jonker

25 (2008) and Small et al. (2009). The stronger horizontal buoyancy gradient (difference between positive and negative buoyancy in Fig 6) generates enhanced turbulence and therefore stronger evaporation. This explains the narrowing of the clouds in the horizontal.

3.2   Cumulus Cloud Field Model Experiments

30 In this section, we explore the effects of thermal radiation on the development of cumulus clouds in the 50 x 50 km^2 domain. Figure 7 provides a first impression of the cumulus cloud field, for three of the six performed simulations. The figure shows a time snapshot at 20 hours of the simulations. The different development of the cloud fields are subject of this section.

Figure 8 shows the temporal development of cloud fraction and maximum liquid water mixing ratio from the restart time until 30 hours. In addition to the 3D and 1D *Thermal radiation* cases, the averaged and fixed radiation scenarios are shown. In the

No-Radiation simulations, cloud cover stays constant at about 10 - 12 % from 8 hours on with a slight decrease towards the end of the simulation. Maximum liquid water mixing ratio is less in the *No-Radiation* simulation, compared to the radiation simulations (1.9 g/kg versus 3.6 g/kg). Differences are found between the *interactive radiation* simulations and the *averaged radiation* simulations. Cloud cover increases more rapidly in the *averaged radiation* simulations compared to the *interactive*

5 ones. The maximum of liquid water mixing ratio, however, shows an opposite development. It is therefore likely that clouds organize differently, depending on the treatment of radiation. The two gray lines at 10 hours and 20 hours indicate stages where the development of the simulation changes. While all radiation simulations perform nearly the same until 10 hours, they start to differentiate afterwards. Maximum liquid water mixing ratio exceeds 2 g/kg after 20 hours. In a rain permitting simulation rain would likely form at that time. We ran the simulations for 30 hours, to see what would theoretically happen to the clouds,

10 but as we are aware that the simulations become more and more unrealistic from 20 hours on, our main analysis will be on the time interval between restart and 20 hours. After 20 hours, a strong increase in cloud fraction in all radiation simulations is found. This increase is particularly strong for the two *averaged radiation* simulations. Looking at the maximum liquid water mixing ratio (and the liquid water path, not shown) an oscillatory behavior of liquid water is found, indicating strong formation of clouds and their decay.

15 Figure 9 shows the temporal development of liquid water path, maximum vertical velocity and cloud base and top height until 20 hours. Liquid water path increases with time in all simulations. The increase is more pronounced in the case of *3D Thermal NCA*. Each of the *interactive* thermal radiation simulations produces more liquid water than its *averaged* counterpart. Liquid water path increases less in the simulation with *constant cooling*. The maximum vertical velocities are weaker in the *No-Radiation* simulation and cloud extend is smaller with a heightened cloud base and lower cloud tops. All quantities increase

20 over time. The different development of the *No-Radiation* simulation and the radiation simulations is related to the missing cooling of the thermal radiation in the *No-Radiation* simulation. Therefore, less water condenses, reducing the number of clouds, cloud cover and a liquid water path. The higher cloud base is also a result of the missing cooling. The smaller increase in cloud top height might be linked to reduced updraft velocities and missing destabilization in the *No-Radiation* simulation (see Section 3.2.1).

25 To study whether the observed differences are simply caused by the systematic bias introduced by 1D or 3D radiation, or if the local effects are relevant, we compare the *averaged* and *interactive* thermal radiation simulations. Although the averaged amount of cooling per domain is (in the beginning of the simulation) the same for both *1D Thermal ICA* and *1D Thermal AVG* (or *3D Thermal NCA* and *3D Thermal AVG*) simulations, the *averaged radiation* simulations produce higher cloud cover than their corresponding 1D or 3D *interactive radiation* simulation. Interestingly, liquid water path and maximum liquid water con-

30 tent is lower for the averaged radiation simulations until 20 hours. The development of all quantities shown here can be related to the location where thermal radiation acts. In the *interactive radiation* simulations, cooling (and some warming at the cloud bottom) acts directly at the cloud edges. Cooling rates can locally be up to several hundred K/d and can destabilize the cloud layer, thus promoting updrafts, more condensation and an increase in cloud height. For the *averaged radiation* simulations, cooling occurs in the cloud layers, but as it is averaged and applied everywhere in a layer, independent of the location of the

35 clouds, a destabilization occurs in the whole area, which is however weaker than the local destabilization of the *interactive*

radiation simulations. Finally, in the constant cooling simulation, the cooling is distributed equally over all heights, cooling in the cloud layer is thus smaller compared to the simulations with radiation which explains the lower liquid water path. This explains the lower values of liquid water. Cooling in the cloud layer, where condensation occurs is reduced in this case.

For both *averaged radiation* simulations, a sudden and strong increase (and decrease) in cloud fraction (and liquid water path, not shown) is found from 22 hours on. This might indicate stronger organization of clouds in the *averaged radiation* simulations after 22 hours of simulations time. However, as stated before, prohibiting the formation of rain leads to unrealistic values of liquid water in this idealized setup of our simulations after 20 hours.

3.2.1 Boundary Layer and Cloud Layer Development

We investigate the development of the boundary layer and cloud layer by examining the profiles of different quantities at three time periods of the simulation. Starting with the initial profile at the restart time (3 hours), we show in addition the averaged profile from 9-11 hours (noted as 10 hours) and from 19-21 hours (noted as 20 hours).

The initial profiles at 3 hours (Fig. 10 and Fig. 11, first row) show the typical profiles of a boundary layer over a warm ocean surface. No clouds have developed yet at this stage. The profile of liquid water potential temperature shows a well mixed layer (up to 400 m), the conditionally unstable layer (up to 1200 m) as well as the inversion layer at about 1100 m height. Relative humidity increases with height at first, before decreasing from 400 m height to the inversion, indicating the entrainment of dry air from aloft the inversion. Typical for the boundary layer over a warm ocean, turbulence is produced by buoyancy in the layer close to the warm ocean (rising thermals). The upward motion of this low layer can also be seen in the updraft velocity in the lower layer until 400 m height (Fig. 11, middle).

The first clouds appear shortly after the restart in all simulations. From this time on, thermal radiation (that is cloud top cooling and cloud bottom warming, and in the case of *3D Thermal NCA* cloud side cooling) changes the development of the boundary layer and of the clouds themselves. Due to the imposed constant surface fluxes of latent and sensible heat, the atmosphere warms over time. When thermal radiation is applied in the simulations, this warming is partially compensated by thermal cooling. At 10 hours, the whole atmosphere is about about 1 K cooler in the thermal radiation simulations (see Fig. 10) which in turn leads to a higher relative humidity and more condensation of water vapor. The increase in liquid water over time was already shown in Fig. 9. Here, in addition to the increased liquid water (which is strongest for the *3D Thermal NCA* radiation case at 10 hours) a deepening of the cloud layer occurs in the simulations including thermal radiation. Thermal cooling at the cloud boundary (*interactive radiation* simulations) and in the cloud layer (*averaged radiation* simulations) cause more condensation. The *constant cooling* simulations produces less water, because the cooling is not directly produced by the clouds but imposed in the simulation setup in the whole atmosphere. Therefore, less cooling is found in the cloud layer compared to the other radiation simulations.

The cooling at cloud tops (and cloud sides in the 3D radiation case) as well as the bottom warming leads to a destabilization of the cloud layer, promoting the development of clouds by increased buoyancy (Figure 11 (second column)). Turbulence that is initially only produced through surface flux induced buoyancy tendencies is now additionally produced in the cloud layer, again

peaking for the *3D Thermal NCA* simulation. Due to the increased buoyancy in the radiation simulations, upward velocities in the clouds are stronger (second column of Fig. 11, middle). Furthermore, all radiation simulations produce stronger downdraft vertical velocities in the subsiding shells, especially the *interactive radiation* simulations (Fig. 11, bottom).

The difference in the temperature profiles between the *No-Radiation* and the radiation simulations increases (up to 3 K), which again, leads to an increase in relative humidity in the sub-cloud layer and more condensation. We note here that in the cloud layer, the relative humidity decreases in the *interactive radiation* simulations. The production of TKE through buoyancy is shifted upward into the cloud layer and upward velocities increase in the cloud layer, which becomes deeper (see the deepening of liquid water profile, Fig. 10). While at the beginning of the simulation, the *3D Thermal NCA* simulations produced the largest amount of liquid water, the averaged radiation simulations produce the largest amount at the end of the simulation. The development of liquid water, relative humidity and the TKE production by buoyancy and the development of vertical velocities suggest that more mixing/entrainment of dry air from aloft the cloud layer occurs in the *interactive radiation* simulations.

We summarize therefore that *1D Thermal* and *3D Thermal* heating and cooling at clouds destabilizes the cloud layer, promoting the development of strong updraft cores and the transport of water vapor into the cloud layer. In addition, the cooling of the atmosphere leads to enhanced condensation. Mixing in the cloud layer is stronger. In addition to the stronger updraft velocities, downdrafts increase as well.

The local cooling at the cloud boundary itself in the *interactive radiation* simulations (in comparison to the *averaged radiation* effect), increases the earlier described development by destabilizing the cloud layer locally at the clouds stronger than in the *averaged radiation* simulations. Entrainment is stronger in the *interactive radiation* simulations, causing less condensation and lower relative humidity. The simulation with *constant cooling* usually shows the weakest effect of all radiation simulations.

We hypothesize that thermal radiation, and in the interactive case, localized thermal heating and cooling (as was already shown for the single cloud simulation) leads to stronger development of the cloud circulation in terms of updrafts and subsiding shells. *3D Thermal NCA* radiation, in comparison to 1D thermal radiation increases these shown effects by an additional cloud side cooling and overall stronger cooling in the modeling domain.

3.2.2 Cloud Development

The preceding section (Sec. 3.2.1) analyzed the effects of thermal radiation on the development of the cloud-topped boundary layer. In this section, we further investigate the effects of thermal radiation on cloud development. It was shown before that the cloud circulation changes due to the effects of thermal radiation, promoting updrafts and subsiding shells, a deepening of the clouds, and depending on the radiation type, increases liquid water within the clouds. Another hypothesis raised earlier is the possible organization of clouds (see beginning of Sec. 3.2) due to thermal radiation. In addition, thermal radiation may alter cloud lifetime. In the following we will address these possible changes.

Cloud Circulation

Results from the single cloud simulation and the statistical analysis of the cloud field simulations suggest that a change in the cloud circulation occurs, promoted by thermal radiative heating and cooling at the clouds. Stronger updrafts and stronger downdrafts/subsiding shells are expected due to the destabilization of the cloud layer and by thermal cooling of the clouds. Therefore, changes in the cloud circulation are expected to be stronger for the simulations with interactive *1D Thermal ICA*

5 and *3D Thermal NCA* radiation, compared to the horizontally *averaged radiation* simulations. All radiation simulations are expected to show stronger circulation features than the *No-Radiation* simulation.

For the cloud field simulations, we used the octant analysis described by Park et al. (2016) to extract updrafts and subsiding shells from our simulations. By the signs of flux perturbations, eight parts (octants) are derived from the spatial field of three variables (vertical velocity and two passive scalars). Those octants include updrafts and subsiding shells. The analysis is re-

10 stricted to cloudy layers (layers, where liquid water mixing ratio is larger than 0.1 g/kg). Figure 12 shows the averaged and maximum updraft and downdraft velocities over time. Updrafts are stronger in all thermal radiation simulations, compared to the *No-Radiation* case. The updraft velocities of the *interactive radiation* simulation are slightly stronger than the updrafts in the *averaged radiation* simulations. The *interactive radiation* simulations produce stronger subsiding shells, noted in the averaged as well as maximum values. Updrafts and downdrafts in the *3D radiation* cases are in general slightly stronger than

15 their *1D* counterparts. Therefore an overall stronger circulation, induced by local heating and cooling is found. These results agree with the increase in buoyancy production, the development of relative humidity and upward vertical velocity as shown in Sec. 3.2.1. In terms of updrafts and subsiding shells we find the *constant cooling* simulations produces similar results as the *averaged radiation* simulations.

20 *Cloud Organization*

Apart from the changes in the cloud circulation, clouds organize differently. Cloud cover and liquid water developed differently for the individual simulations. The horizontally *averaged radiation* simulations showed a larger cloud cover over time than the *interactive radiation* simulations.

To investigate how the cloud structures change over time, we calculated the temporal variation in the autocorrelation length

25 (defined by the shift where the correlation coefficient drops below 1/e) from the liquid water path of the cloud field (Fig. 13). Autocorrelation is a measure for the size of the clouds. At about 9 hours, the simulations start to develop differently. Both *interactive radiation* simulations show an increased correlation length from this time on, indicating stronger organization of the clouds. The largest cloud patches are found for the *3D Thermal NCA* simulation. Both *averaged radiation* simulations simulation behave quite similar and show less organization than the *interactive radiation* simulations, but slightly more than

30 the *No-Radiation* simulation. The *constant cooling* simulation is located between the *averaged radiation* simulations and the *No-Radiation* simulation.

It shall be mentioned here (although not shown) that from about 24 hours on, strong organization occurs in the *averaged radiation* simulations and the *const cooling* simulation, in which the clouds oscillate: disappearing and then reappearing. No systematic difference between 1D and 3D radiation is found in these cases.

35 To further investigate how much water the individual clouds contain and if and how they organize, we show hovmoeller di-

agrams (Fig. 14). Liquid water path was averaged in x-direction for these diagrams. They thus provide an overview of the spacial and temporal development of the cloud field. Extended patches of liquid water along the spacial dimensions indicate large clouds. Extended patches along the time axis show long living clouds. In additions, the diagrams show how much water is located in the cloud patches.

5 In the *No-Radiation* simulation, no organization occurs. Clouds remain small with little liquid water content throughout the simulation. This is different if thermal radiation is accounted for. If we compare the five different radiation simulations, one notices that both *interactive radiation* simulations and both horizontally *averaged radiation* simulations as well as the *constant cooling* simulation show a similar behavior.

Larger structures with more liquid water content form much earlier in the simulations with *interactive thermal radiation*.
10 Patches of dry and wet regions form (blue till red vs. white areas) and the cloud patterns in the *interactive radiation* simulations contain more liquid water and show larger structures. The simulations with the horizontally *averaged radiation* also show growing structures but they contain less liquid water and are smaller during the shown simulation time. Also, no significant differences exists between the 1D and 3D *averaged radiation* simulations (which was also evident in Fig. 13). Comparing the 1D and 3D *interactive thermal radiation* simulations, we find larger structures earlier in the *3D Thermal NCA* radiation simula-
15 tion. Also, clouds in the *interactive radiation* simulations contain more liquid water. The fiber-like structures of the hovmoeller diagrams usually give a hint on the movement of the clouds. Here, however, the structures show that clouds move very little during their lifetime and mostly remain at one location, as our simulation is performed without any background mean wind.

We can therefore summarize the following findings: Interactive thermal radiation enhances cloud organization in our simulations in the first 20 hours.
20 For a matter of completeness, it shall be mentioned that strong organization occurs after 24 hours in the *averaged radiation* simulations, exceeding the cloud organization in the *interactive radiation* simulations.

Cloud Lifetime

Radiation may, in addition to the previously shown changes, alter the cloud's lifetime and size. Figure 15 shows a probability
25 density function (pdf) of cloud lifetime. Each cloud occurring within the first 20 hours of our simulations was tracked and the lifetime was calculated. *Interactive thermal radiation* leads to less clouds with a small lifetime, but more clouds with a larger lifetime. This result agrees with our previous findings: Enhanced turbulence and mixing in the *interactive radiation* simulations can lead to a faster decay of small clouds, while larger clouds might live longer and grow due to the enhanced cloud circulation (stronger updrafts and downdrafts). The *averaged radiation* simulations show more clouds with a longer lifetime
30 than the *No-Radiation* and the *const. cooling* case.

Figure 16 shows the pdf compared to simulation time and the cloud size. Many small clouds occur at the beginning of the simulations. In the *interactive radiation* simulations, these small clouds become fewer over time and more larger clouds occur, while in all other simulations, these small clouds occur throughout the whole simulation. Clouds larger than $1\ 10^3$ km^2 occur
35 in the *interactive radiation* simulations, but hardly any in the *No-Radiation* and the *const. cooling* case.

3.2.3 Dependence of the Results on Resolution and Reproducibility

One important issue of our simulations is the robustness of the results and the dependence on resolution. We therefore repeated the calculation with a resolution of 100 m instead of 50 m and performed three runs for the computationally cheaper 100 m resolution. Although small differences are found in the statistical analysis of profiles and time series of the different variables

5   the organization effect remains. Figures. 17 and 18 show the hovmoeller diagrams and autocorrelation length, this time calculated from the 100 m resolution simulations. Again clouds start organizing earlier if *interactive radiation*, especially the 3D *interactive radiation* is accounted for. The separation into moist and dry regions is stronger in the simulation with a coarser resolution. The clouds of the interactive radiation simulations also contain more liquid water, similar to the 50 m resolution simulations. The effects of 3D *Thermal radiation* is even larger than in the 50 m resolution case. Due to the reduced resolution,

10 this simulation is computationally less expensive and we repeated it two times. Although small differences occur (one reason being for example the randomly chosen spectral bands in the MCSI), the effects (e.g. stronger organization or the more locally focused liquid water in the 3D *interactive radiation* radiation case) remain the same.

4   Conclusions

15 We found that thermal radiation affects cloud development. This was first investigated for idealized single clouds induced by a heat bubble perturbation close to the surface as well as for idealized simulations of cumulus cloud fields. Thermal radiation changes the cloud circulation which includes stronger updraft vertical velocities and stronger subsiding shells around the clouds. Overall, we find an increased mixing and entrainment in the simulations with radiation. Both, the mixing and the resulting vertical velocities are due to a destabilization of the atmosphere which results from thermal cooling.

20 The change in the overall dynamics causes clouds to organize. Clouds also become deeper in vertical extent and contain more liquid water if thermal radiation is accounted for.

One important objective of our simulations was to investigate the effect of 3D *interactive* thermal radiation. Therefore, we performed four different thermal radiation simulations. We separate between 1D and 3D thermal radiation as well as between *interactive* and *averaged* radiation. We find that the effects described above are always stronger if 3D thermal radiation is

25 applied, compared to 1D thermal radiation. Differences in the overall development of the cloud field are evident between the *interactive* and *averaged* radiation application. The most pronounced difference between the *interactive* and *averaged* radiation simulations is the development of cloud organization. Organization starts earlier if *interactive radiation* is applied. If the simulations are run beyond 20 hours larger cloud structures form in the simulations with *averaged radiation*, exceeding the cloud sizes in the *interactive* radiation simulations.

30 The main difference between the *averaged* and the *interactive radiation* is the location and the strength of the thermal cooling. In the case of *interactive radiation*, the cooling (or heating) acts locally at the cloud sides, tops and bottom. Cooling rates can be as large as several 100 K/d. This causes a local destabilizing. This is supported by stronger updrafts and downdrafts for the *interactive radiation* simulations. In case of the *averaged radiation*, the resulting cooling is weaker but acts in the entire

modeling domain and the cooling does not distinguish between cloudy and cloudless regions. It therefore takes longer for the *averaged radiation* to destabilize the atmosphere. However, when a certain destabilization is reached , it causes a rapid cloud development in the entire domain at once (like in our simulations after 20 hours). This might explain why cloud organization starts earlier in the case of *interactive radiation*, but that cloud organization are eventually larger for the *averaged radiation*

5 case, if the simulation is run long enough. Fig. 19 summarizes our findings. The main findings of our study are reproducible at coarser horizontal resolution and with perturbed initial conditions.

Obviously, the simulations shown in this study are in an idealized framework to omit feedback mechanisms which would occur otherwise. The fixed surface fluxes omit the surface flux feedback which was found e.g. by Muller and Held (2012) who proposed that this could be a reason for the organization of clouds. Another feedback mechanism which we neglect is the effect

10 of rain and possible cold pool dynamics. Cold pool dynamics are usually associated with cloud organization (e.g. Seifert and Heus (2013)). This cannot be the cause for the cloud organization which we find in our simulations and with our setup we isolated the radiation effects. However, it is obvious that the clouds produced in our simulations are deep enough to cause rain from about 20 hours on, if we would allow it. If we would account for rain effects, the whole system would possibly change. Rain would set in earlier in all thermal radiation simulations (compared to the *No-Radiation* case), and most likely earlier in

15 the *interactive radiation* simulations. We rerun the *1D ICA interactive radiation* simulations, allowing for rain, and found rain to occur after 22 hours. In a more realistic framework (e.g. simulations allowing for rain or surface interaction), it is not certain that we would ever reach the stage where clouds organize in the *averaged radiation* simulations, but we may reach the stage in the *interactive* ones. Furthermore, in a more realistic setup, one would have to account for solar radiative effects as well, not only for thermal radiative effects.

20 Previous studies (Emanuel et al. (2014), Muller and Held (2012), Muller and Bony (2015)) used RCE experiments and found thermal radiation to be a key driver for cloud organization. Our simulations are for a much smaller domain, with higher spatial resolution, and without deep convection. Yet, we also find that thermal radiation is a driver for organization. Also, our simulations show that it might be essential how radiative transfer is applied. The effects of *interactive* and *averaged* application of radiation differs significantly. In addition 3D, *interactive radiation* and the thus additional local cooling at cloud

25 sides changes the cloud development stronger than 1D *interactive radiation* (e.g. downdrafts or organization). The differences between a 1D and 3D *averaged radiation* application is, in contrast to the differences between 1D and 3D *interactive radiation* simulations, small.

Appendix A: Simulation Setup

Table 1 and 2 provide input data for the heat bubble and cumulus cloud field simulation.

30 *Acknowledgements.* This work was funded by the Federal Ministry of Education and Research (BMBF) through the High Definition Clouds and Precipitation for Climate Prediction (HD(CP)[2]) project (FKZ: 01LK1208A), HD(CP)[2] phase 2 (FKZ: 01LK1504D) and the DFG Tran-

Model Variables	Value
Number of Grid Boxes	64 x 64
Number of z-levels	70
Resolution	100 m
Vertical Stretching	10 %
Surface Forcing	0.8 K
SST	288 K
CCN	$70 \cdot 10^6 \ 1/dm^3$
Microphysics	warm, no rain
Variable Output	every 100 s
Surface Type	fixed SST

Table 1. Model setup for the heat bubble simulations.

Model Variables	SC_field
Number of Grid Boxes	256 x 256
Number of z-levels	110
Resolution x,y	100 m
Resolution z	30 m
Vertical Stretching	10 %
CCN	$150 \cdot 10^6 \ 1/dm^3$
Microphysics	warm, no rain
Variable Output	every 300 s
Surface Fluxes	prescribed
Latent Heat	180 W/m^2
Sensible Heat	18 W/m^2
Restart	10800 s

Table 2. Model input for cumulus simulations.

sregio 165 "Waves to Weather". We thank George Craig for very helpful suggestions for the setup of the model experiments and the interpretation of the data. Many thanks go to DKRZ, Hamburg, for providing us with the computational resources.

References

Bellon, G. and Geoffroy, O.: Stratocumulus radiative effect, multiple equilibria of the well-mixed boundary layer and transition to shallow convection, Quarterly Journal of the Royal Meteorological Society, 142, 1685–1696, doi:10.1002/qj.2762, http://dx.doi.org/10.1002/qj.2762, 2016a.

Bellon, G. and Geoffroy, O.: How finely do we need to represent the stratocumulus radiative effect?, Quarterly Journal of the Royal Meteorological Society, 142, 2347–2358, doi:10.1002/qj.2828, http://dx.doi.org/10.1002/qj.2828, 2016b.

Bony, S., Stevens, B., Frierson, D. M. W., Jakob, C., Kageyama, M., Pincus, R., Shepherd, T. G., Sherwood, S. C., Siebesma, A. P., Sobel, A. H., Watanabe, M., and Webb, M. J.: Clouds, circulation and climate sensitivity, Nature Geosci, 8, 261–268, 2015.

Boucher, O., Randall, D., Artaxo, P., Bretherton, C., Feingold, G., Forster, P., Kerminen, V.-M., Kondo, Y., Liao, H., Lohmann, U., Rasch, P., Satheesh, S., Sherwood, S., Stevens, B., and Zhang, X.: Clouds and aerosols. In Climate Change 2013: The Physical Science Basis. Contribution of Working Group I to the Fifth Assessment Report of the Intergovernmental Panel on Climate Change., pp. 571–657, Cambridge University Press, 2013.

Brewster, M.: Evaporation and condensation of water mist/cloud droplets with thermal radiation, International Journal of Heat and Mass Transfer, 88, 695 – 712, doi:http://dx.doi.org/10.1016/j.ijheatmasstransfer.2015.03.055, http://www.sciencedirect.com/science/article/pii/S0017931015003130, 2015.

Cahalan, R., Oreopoulos, L., Marshak, A., Evans, K., Davis, A., Pincus, R., Yetzer, K., Mayer, B., Davies, R., Ackerman, T., H.W., B., Clothiaux, E., Ellingson, R., Garay, M., Kassianov, E., Kinne, S., Macke, A., O'Hirok, W., Partain, P., Prigarin, S., Rublev, A., Stephens, G., Szczap, F., Takara, E., Varnai, T., Wen, G., and Zhuraleva, T.: The International Intercomparison of 3D Radiation Codes (I3RC): Bringing together the most advanced radiative transfer tools for cloudy atmospheres, Bulletin of the American Meteorological Society, 86, 1275–1293, 2005.

Cheng, A., Xu, K.-M., and Stevens, B.: Effects of Resolution on the Simulation of Boundary-layer Clouds and the Partition of Kinetic Energy to Subgrid Scales, Journal of Advances in Modeling Earth Systems, 2, 2010.

Davies, R. and Alves, A.: Flux divergence of thermal radiation within stratiform clouds, Journal of Geophysical Research, 94, 16 277–16 286, 1989.

de Lozar, A. and Muessle, L.: Long-resident droplets at the stratocumulus top, Atmos. Chem. Phys., 16, 6563–6576, doi:10.5194/acp-16-6563-2016, http://www.atmos-chem-phys.net/16/6563/2016/, 2016.

Emanuel, K., Wing, A. A., and Vincent, E. M.: Radiative-convective instability, Journal of Advances in Modeling Earth Systems, 6, 75–90, doi:10.1002/2013MS000270, http://dx.doi.org/10.1002/2013MS000270, 2014.

Fu, Q. and Liou, K.: On the correlated k-distribution method for radiative transfer in nonhomogeneous atmospheres, Journal of the Atmospheric Sciences, 49, 2139–2156, 1992.

Fu, Q., Krueger, S., and Liou, K.: Interactions of radiation and convection in simulated tropical cloud clusters, Journal of the Atmospheric Sciences, 52, 1310–1328, 1995.

Guan, H., Davies, R., and Yau, M.: Longwave radiative cooling rates in axially symmetric clouds, Journal of Geophysical Research, 100, 3213–3220, 1995.

Guan, H., Yau, M., and Davies, R.: The Effects of Longwave Radiation in a Small Cumulus Cloud, Journal of the Atmospheric Sciences, 54, 2201–2214, 1997.

Harrington, J., Feingold, G., and Cotton, W.: Radiative Impacts on the Growth of a Population of Drops within Simulated Summertime Arctic Stratus, Journal of the Atmospheric Sciences, 57, 766–785, 2000.

Hartman, C. and Harrington, J.: Radiative impacts on the growth of drops within simulated marine stratocumulus. Part I: Maximum solar heating, Journal of the Atmospheric Sciences, 62, 2323–2338, 2005a.

Hartman, C. and Harrington, J.: Radiative impacts on the growth of drops within simulated marine stratocumulus. Part II: Solar zenith angle variations, Journal of the Atmospheric Sciences, 62, 2339–2351, 2005b.

Heus, T. and Jonker, H. J. J.: Subsiding shells around shallow cumulus clouds, Journal of the Atmospheric Sciences, 65, 1003–1081, 2008.

Jakub, F. and Mayer, B.: 3-D radiative transfer in large-eddy simulations – experiences coupling the TenStream solver to the UCLA–LES, Geoscientific Model Development Discussions, 8, 9021–9043, doi:10.5194/gmdd-8-9021-2015, 2015.

Jiang, H., Xue, H., Teller, A., Feingold, G., and Levin, Z.: Aerosol effects on the lifetime of shallow cumulus, Geophysical Research Letters, 33, l14806, 2006.

Kablick, G., Ellingson, R., Takara, E., and Gu, J.: Longwave 3D Benchmarks for Inhomogeneous Clouds and Comparisons with Approximate Methods, Journal of Climate, 24, 2192–2205, 2011.

Klinger, C. and Mayer, B.: Three-dimensional Monte Carlo calculation of atmospheric thermal heating rates , Journal of Quantitative Spectroscopy and Radiative Transfer, 144, 123 – 136, doi:http://dx.doi.org/10.1016/j.jqsrt.2014.04.009, 2014.

Klinger, C. and Mayer, B.: The Neighboring Column Approximation (NCA) –- A fast approach for the calculation of 3D thermal heating rates in cloud resolving models , Journal of Quantitative Spectroscopy and Radiative Transfer, 168, 17 – 28, doi:http://dx.doi.org/10.1016/j.jqsrt.2015.08.020, http://www.sciencedirect.com/science/article/pii/S0022407315002964, 2016.

Larson, V. E., Fleishauer, R. P., Kankiewicz, J. A., Reinke, D. L., and Vonder Haar, T. H.: The death of an altocumulus cloud, Geophysical Research Letters, 28, 2609–2612, 2001.

Lilly, D. K.: Cirrus Outflow Dynamics, Journal of the Atmospheric Sciences, 45, 1594–1605, doi:10.1175/1520-0469(1988)045<1594:COD>2.0.CO;2, http://dx.doi.org/10.1175/1520-0469(1988)045<1594:COD>2.0.CO;2, 1988.

Liou, K.-N., Fu, Q., and Ackerman, T.: A simple formulation of the delta-four-stream approximation for radiative transfer parameterizations, Journal of the Atmospheric Sciences, 45, 1940–1947, 1988.

Marquis, J. and Harrington, J.: Radiative influences on drop and cloud condensation nuclei equilibrium in stratocumulus, Journal of Geophysical Research, 110, doi:10.1029/2004JD005 401, 2005.

Mayer, B.: Radiative transfer in the cloudy atmosphere, European Physical Journal Conferences, 1, 75–99, doi:10.1140/epjconf/e2009-00912-1, 2009.

Muller, C. and Bony, S.: What favors convective aggregation and why?, Geophysical Research Letters, 42, 5626–5634, 2015GL064260, 2015.

Muller, C. J. and Held, I. M.: Detailed investigation of the self-aggregation of convection in cloud-resolving simulations, Journal of the Atmospheric Sciences, 69, 2551–2565, 2012.

Park, S., Gentine, P., Schneider, K., and Farge, M.: Coherent Structures in the Boundary and Cloud Layers: Role of Updrafts, Subsiding Shells, and Environmental Subsidence, Journal of the Atmospheric Sciences, 73, 1789–1814, doi:10.1175/JAS-D-15-0240.1, 2016.

Petters, J., Harrington, J., and Clothiaux, E.: Radiative˘dynamical feedbacks in low liquid water path stratiform clouds, Journal of the Atmospheric Sciences, 69, 1498–1512, 2012.

Pincus, R. and Stevens, B.: Monte Carlo spectral integration: A consistent approximation for radiative transfer in large eddy simulations, Journal of Advances in Modeling Earth Systems, 1, 2009.

Seifert, A. and Beheng, K. D.: A double-moment parameterization for simulating autoconversion, accretion and self collection, Atmos. Res., 59-60, 256–382, 2001.

Seifert, A. and Heus, T.: Large-eddy simulation of organized precipitating trade wind cumulus clouds, Atmos. Chem. Phys., 13, 5631–5645, doi:10.5194/acp-13-5631-2013, http://www.atmos-chem-phys.net/13/5631/2013/, 2013.

5 Small, J., Chuang, Y., Feingold, G., and Jiang, H.: Can aerosol decrease cloud lifetime?, Geophysical Research Letters, 36, 116806, 2009.

Sommerai, G.: Three-dimensional simulation of turbulent processes in an undisturbed trade wind boundary layer, Journal of the Atmospheric Sciences, 33, 216–241, 1976.

Stevens, B.: On the growth of layers of non-precipitating cumulus convection, J. Atmos. Sci, 64, 2916–2931, 2007.

Stevens, B., Moeng, C., Ackerman, A., Bretherton, C., Chlond, A., De Roode, S., Edwards, J., Golaz, J., Jiang, H., Khairoutdinov, M.,
10   Kirkpatrick, M., Lewellen, D., Lock, A., Muller, F., Stevens, D., Whelan, E., and Zhu, P.: Evaluation of large-eddy simulations via observations of nocturnal marine stratocumulus, Mon. Weather Rev., 133, 1443–1462, 2005.

Tao, W.-K., Simpson, J., Sui, C. H., Ferrier, B., Lang, S., Scala, J., Chou, M. D., and Pickering, K.: Heating, moisture, and water budgets of tropical and midlatitude squall lines: comparisons and sensitivity to longwave radiation, Journal of the Atmospheric Sciences, 50, 673–690, 1993.

15 Tao, W.-K., Lang, S., Simpson, J., Sui, C. H., Ferrier, B., and Chou, M. D.: Mechanisms of cloud-radiation interaction in the tropics and midlatitudes, Journal of the Atmospheric Sciences, 53, 2624–2651, 1996.

van Zanten, M., Stevens, B., Nuijens, L., Siebesma, A., Ackerman, A., Burnet, F., Cheng, A., Couvreux, F., Jiang, H., Khairoutdinov, M., Kogan, Y., Lewellen, D., Mechem, D., Nakamura, K., Noda, A., Shipway, B., Slawinska, J., Wang, S., and Wyszogrodzki, A.: Controls on precipitation and cloudiness in simulations of trade-wind cumulus as observed during RICO, J. Adv. Model. Earth Syst., 3, 2011.

20 Xiao, H., Gustafson, W. I., and Wang, H.: Impact of subgrid-scale radiative heating variability on the stratocumulus-to-trade cumulus transition in climate models, Journal of Geophysical Research: Atmospheres, 119, 4192–4203, doi:10.1002/2013JD020999, http://dx.doi.org/10.1002/2013JD020999, 2014.

Xu, K.-M. and Randall, D. A.: Impact of interactive radiative transfer on the macroscopic behavior of cumulus ensembles. Part II: Mechanisms for cloud-radiation interactions., Journal of the Atmospheric Sciences, 52, 800–817, 1995.

25 Zinner, T., Mannstein, H., and Tafferner, A.: Cb-TRAM: Tracking and monitoring severe convection from onset over rapid development to mature phase using multi-channel Meteosat-8 SEVIRI data, Meteorology and Applied Physics, pp. doi:10.1007/s00703–008–0290–y, 2008.

List of Figures

Figure 1. Three dimensional heating and cooling rates and surface fluxes in a cumulus cloud field, calculated with the Monte Carlo model MYSTIC (Mayer, 2009; Klinger and Mayer, 2014).

Figure 2. Visualization of the four single cloud simulations (first: weak symmetric; second: weak non-symmetric; third: strong symmetric; fourth:strong non-symmetric). The snap shot of the cloud field is taken at 20 min of the simulation of the *No-Radiation* case. The visualization was performed with the 3D radiative transfer model MYSTIC (Mayer, 2009). The clouds in the background are a feature of the visualization and do not occur in the LES simulation of the single clouds.
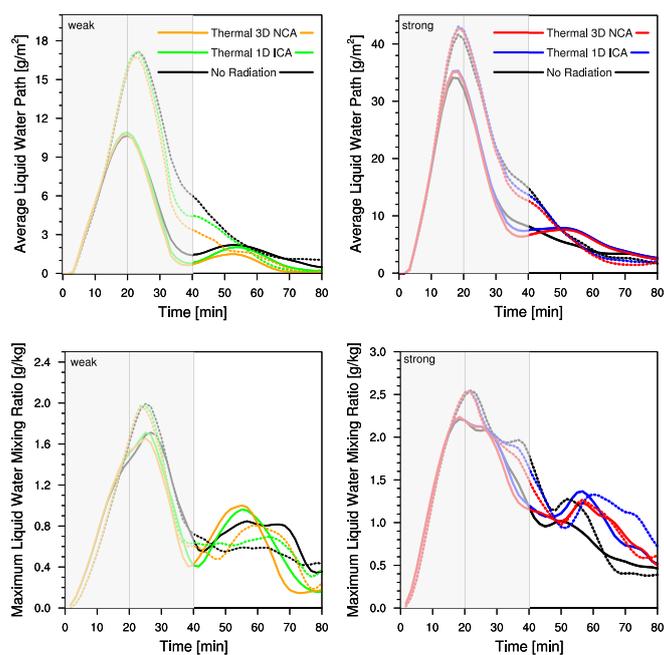
Figure 3. Time development of conditionally sampled liquid water path and maximum liquid water mixing ratio for the simulations of the single clouds. Only liquid water belonging to the single cloud was considered. The left column shows the weaker forced, the right column the stronger forced single clouds. Solid lines represent the non-symmetric cloud, dashed lines the symmetric cloud.
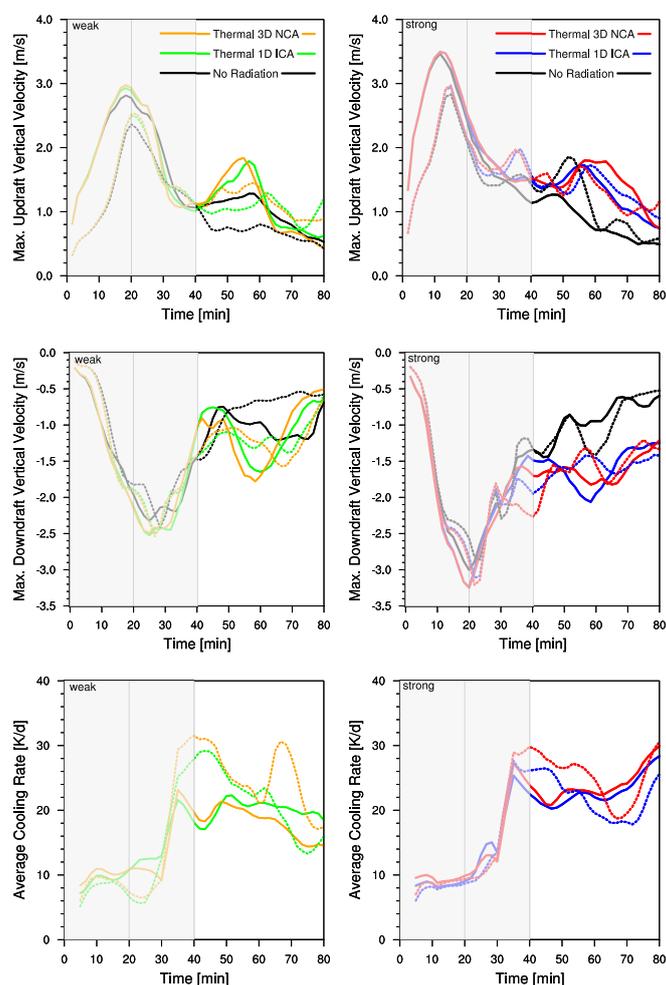
Figure 4. Time development of maximum updraft and downdraft vertical velocity as well as conditionally sampled cooling rates of the single cloud simulations for the simulations of the single clouds. Cooling rates were sample at the single cloud only. The left column shows the weaker forced, the right column the stronger forced single clouds. Solid lines represent the non-symmetric cloud, dashed lines the symmetric cloud.
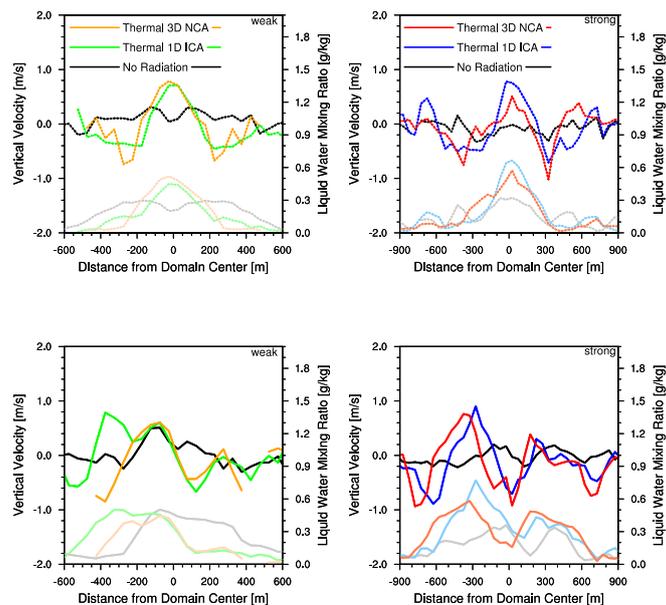
Figure 5. Height and time averaged transects of liquid water mixing ratio (pale color, bottom, right axis) and vertical velocity (middle, left axis). The time average was performed over 3 min at around 60 min simulations time. The vertical average was taken in the middle of the vertical extend of the cloud to cover cloud side areas. Dashed lines show the symmetric cloud, solid lines the non-symmetric cloud.
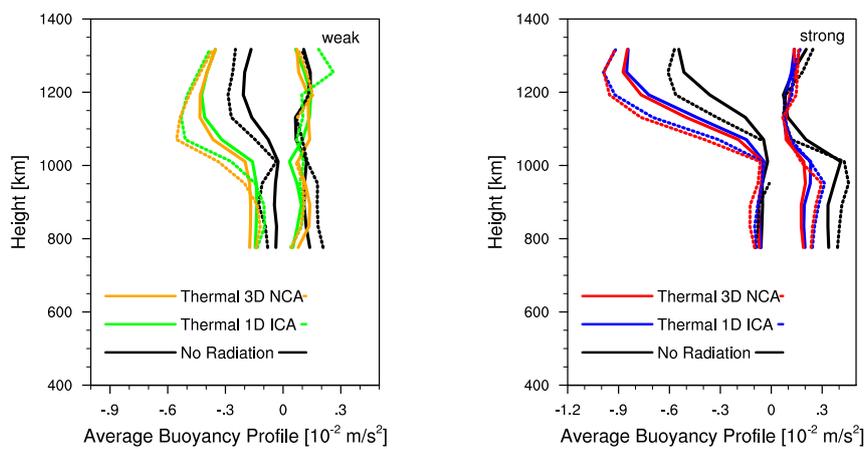
Figure 6. Positive and negative buoyancy profile sampled at 50-58 min of the simulation in the cloudy area. Dashed lines show the symmetric cloud, solid lines the non-symmetric cloud.
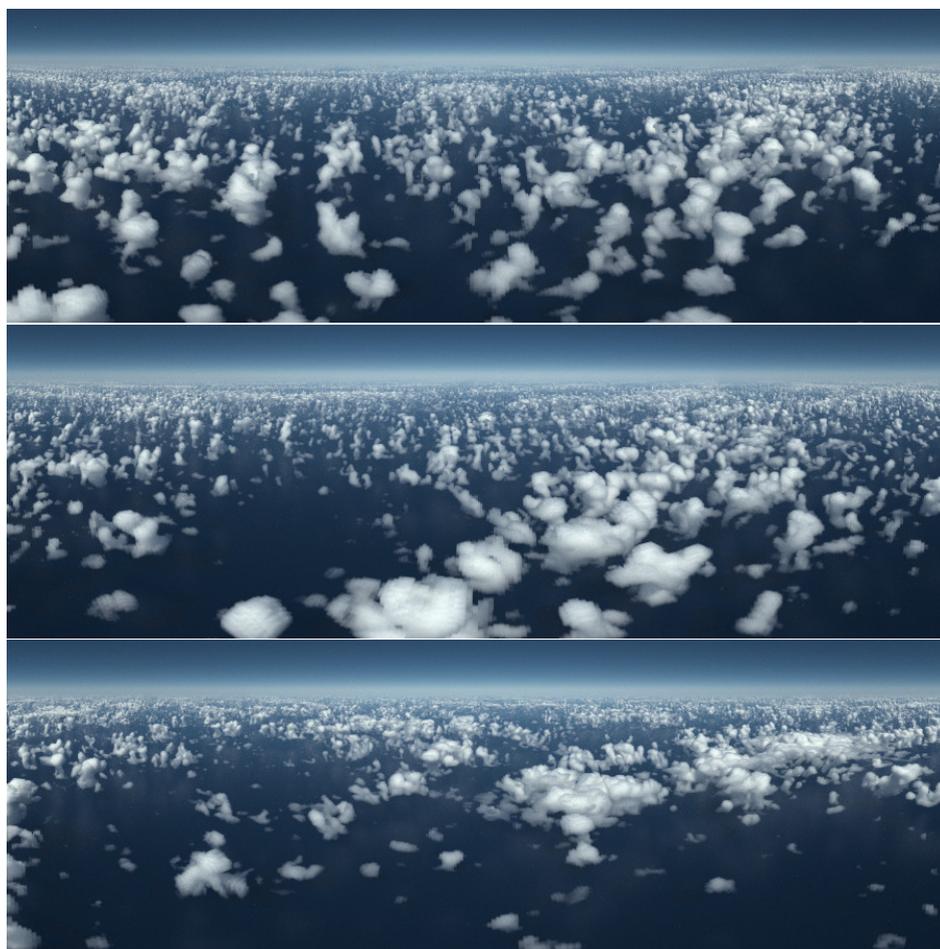
Figure 7. Visualization of the cumulus cloud field of the *constant cooling* (top), *3D Thermal Average* (middle) and *3D Thermal NCA* (bottom) simulations. The snap shot of the cloud field is taken at 20 hours of the simulation. The visualization was performed with the 3D radiative transfer model MYSTIC (Mayer, 2009).
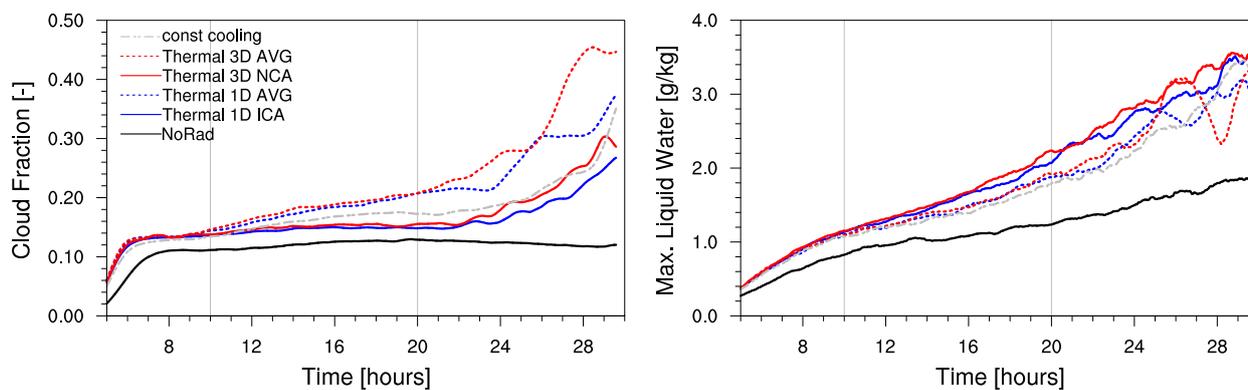
Figure 8. Time development of cloud fraction and maximum liquid water mixing ratio from 5 to 30 hours. The two gray lines (at 10 hours and 20 hours) separate the development in different periods for the further analysis.
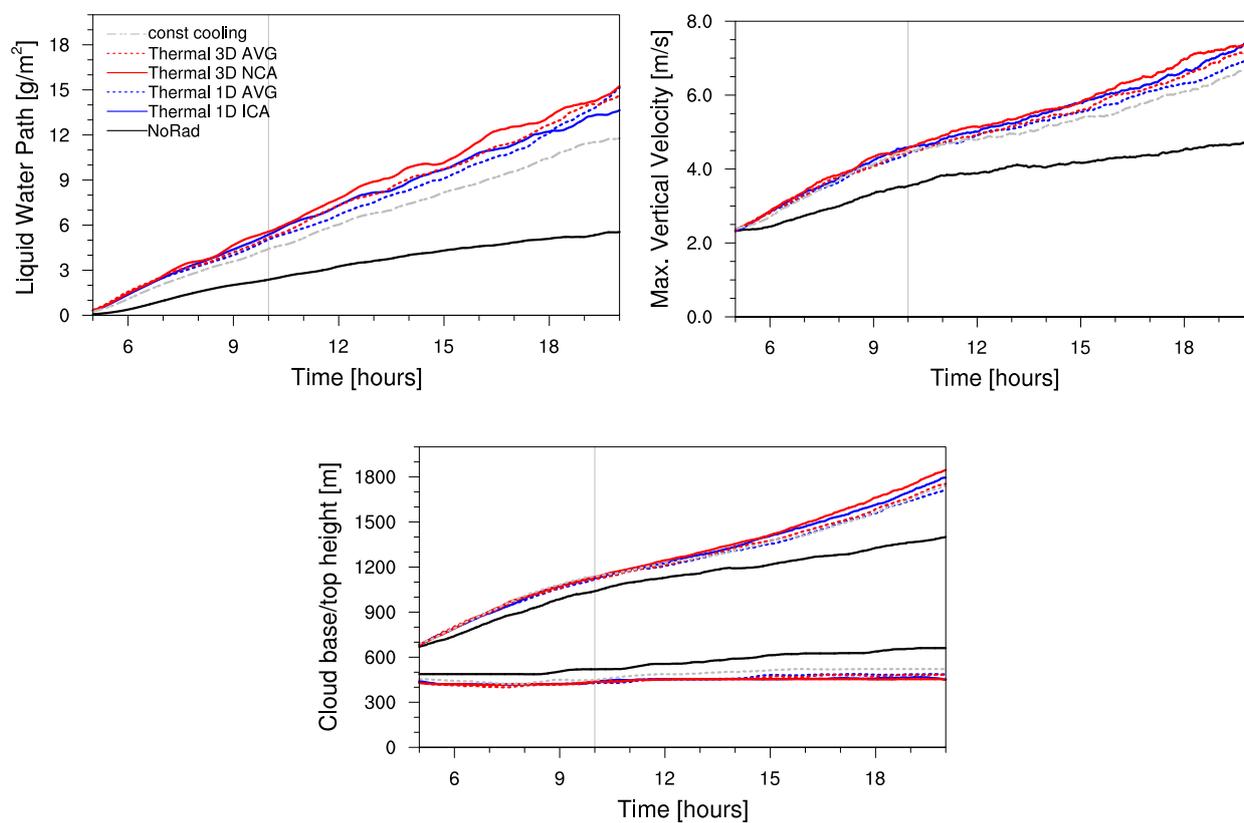
Figure 9. Time development of liquid water path, maximum vertical velocity and cloud base and cloud top height. The gray line (at 10 hours) separates the development in different periods for the further analysis.
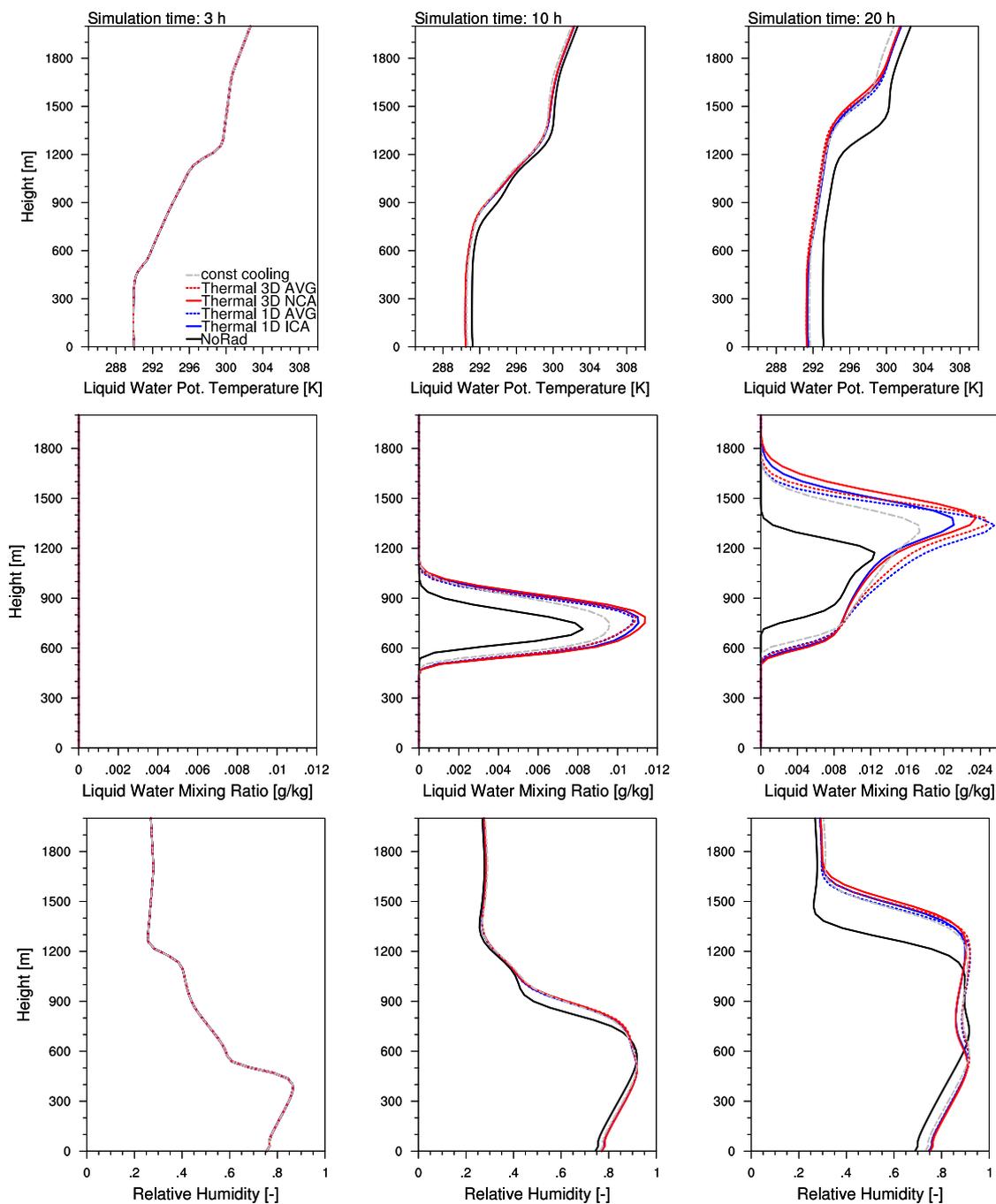
Figure 10. Time averaged profiles of liquid water potential temperature, liquid water mixing ratio and relative humidity. The profiles are shown at the restart time (3 hours), as an 3 hour averaged around 10 hours and 20 hours of the simulations.
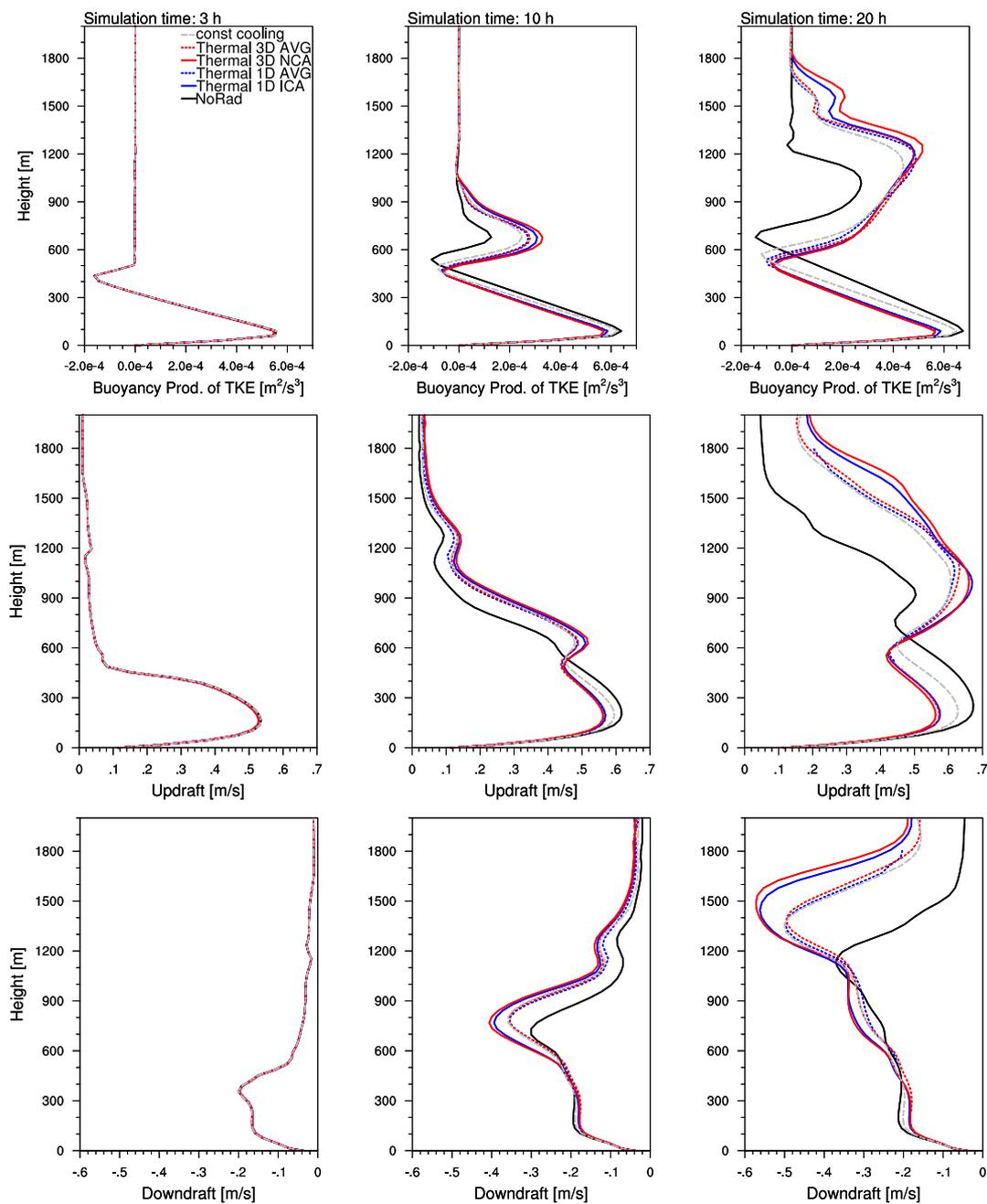
Figure 11. Time averaged profiles of buoyancy production of the TKE and updraft and downdraft vertical velocity. The profiles are shown at the restart time (3 hours), as an 3 hour averaged around 10 hours and 20 hours of the simulations. Updraft and downdraft vertical velocities were extracted from the 3D data following Park et al. (2016)
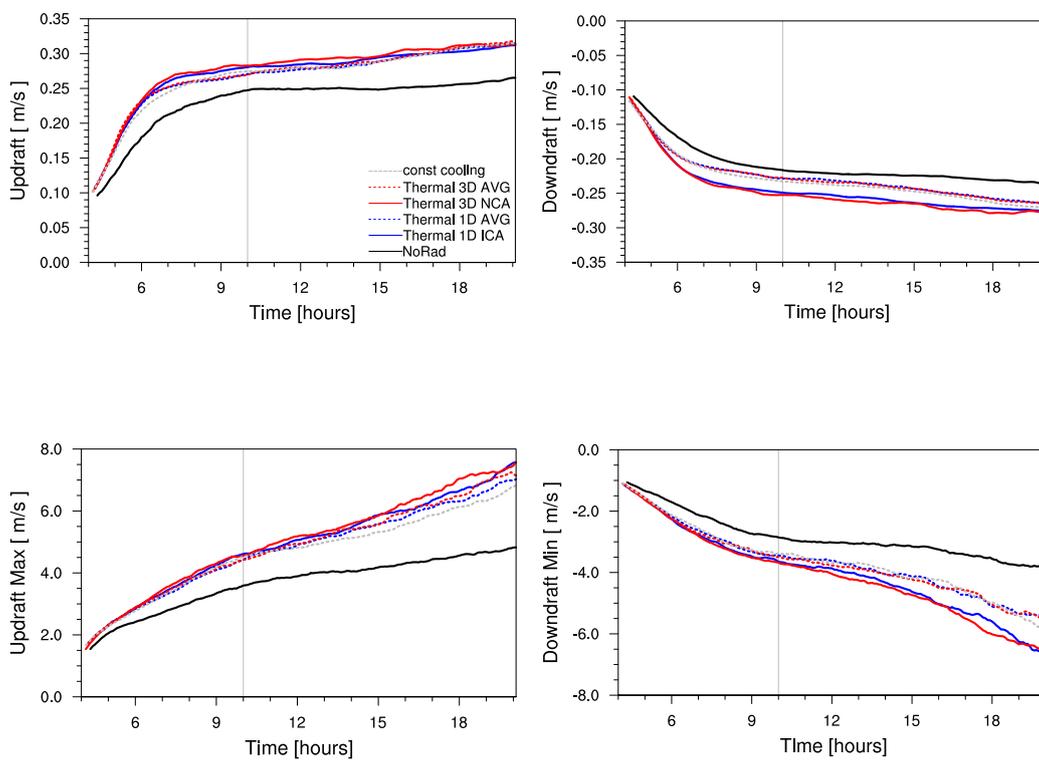
Figure 12. Time series of averaged vertical velocity as well as maximum updraft and downdraft vertical velocity of updrafts and downdrafts.
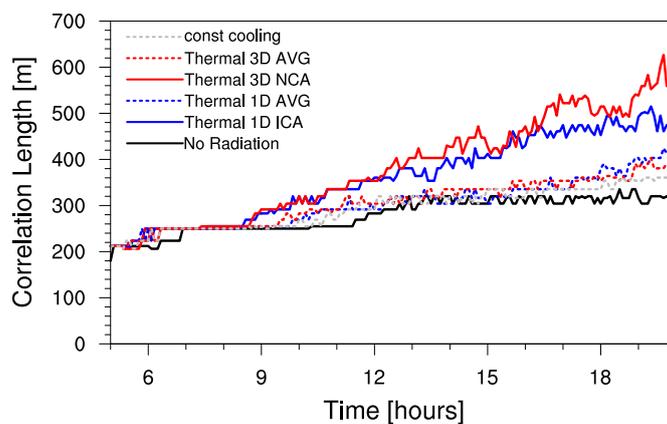
Figure 13. Time development of correlation length. The correlation length is defined by the shift where the correlation coefficient drops below 1/e.
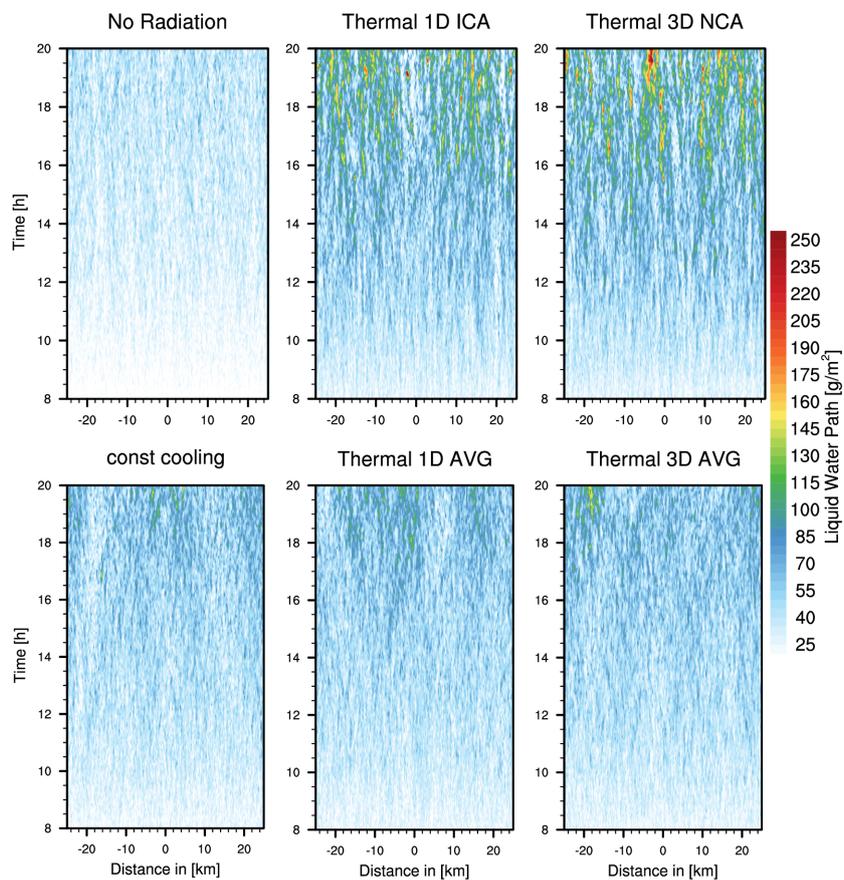
Figure 14. Hovmoeller Diagram of liquid water path, averaged in x-direction.
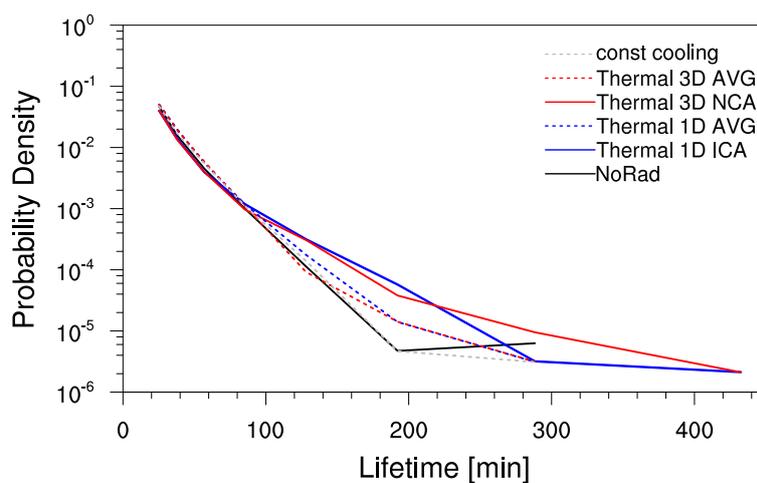
Figure 15. Probability density function of cloud lifetime: The lifetime of each cloud detected by the tracking algorithm was calculated within the first 20 hours of the simulations.
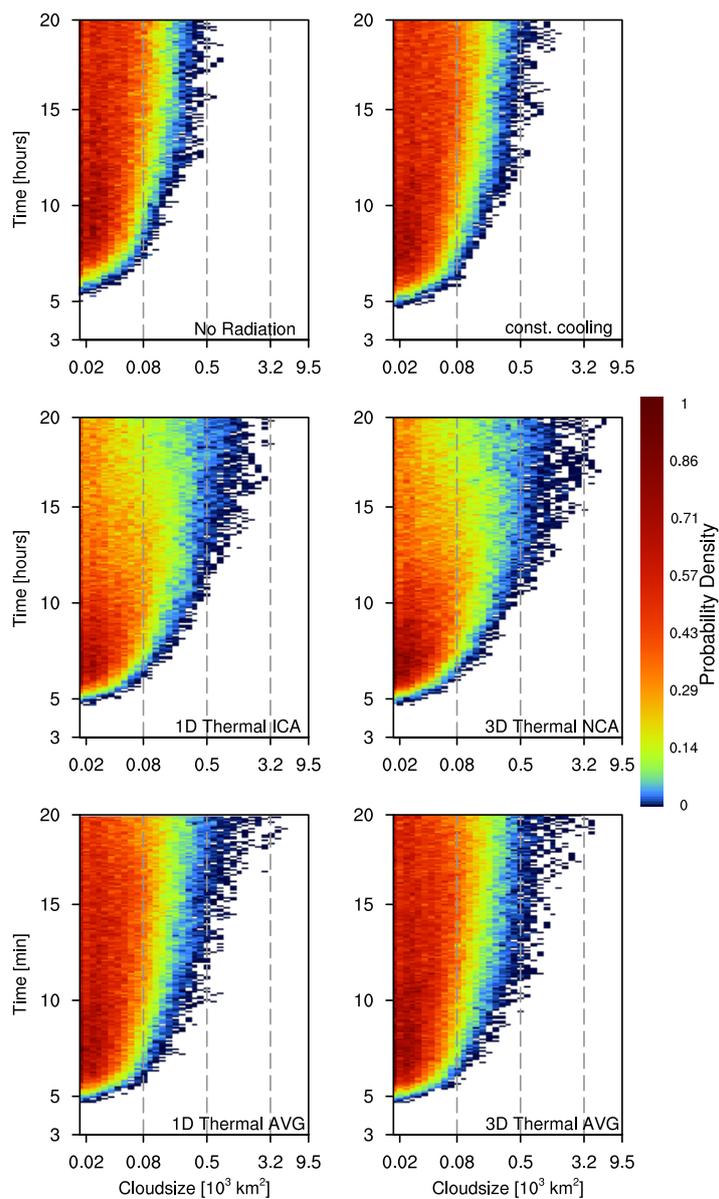
Figure 16. Probability density with respect to cloud size and the time of occurrence in the different simulations.
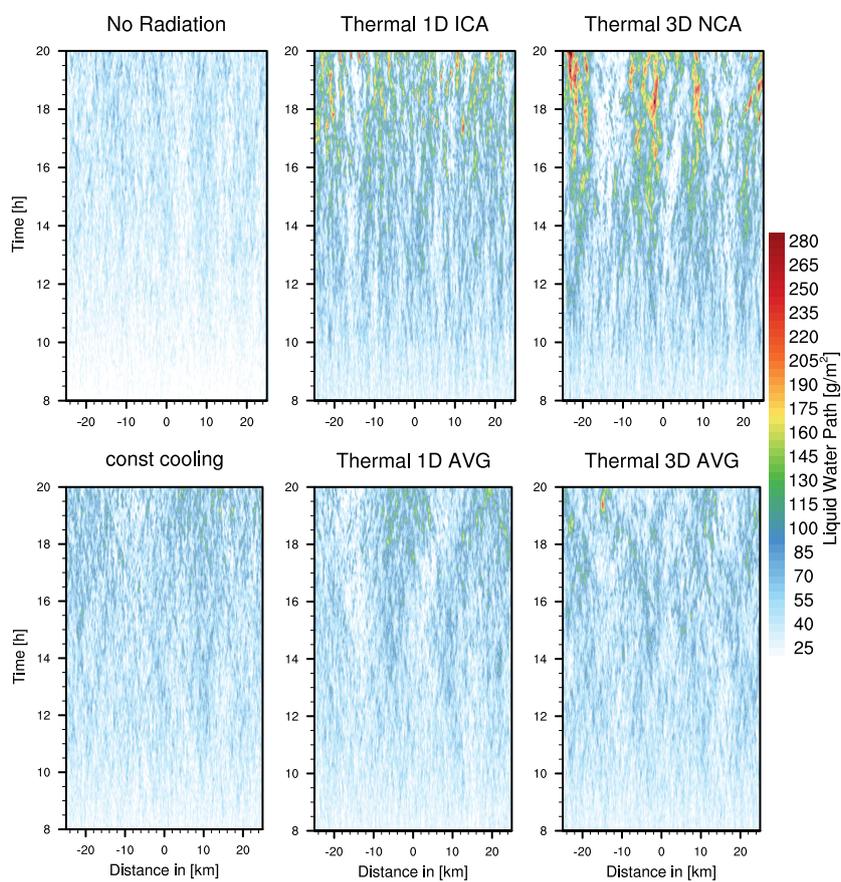
Figure 17. Cloud organization in the 100 m resolution simulations shown as hovmoeller diagrams of the liquid water path, averaged in x-direction
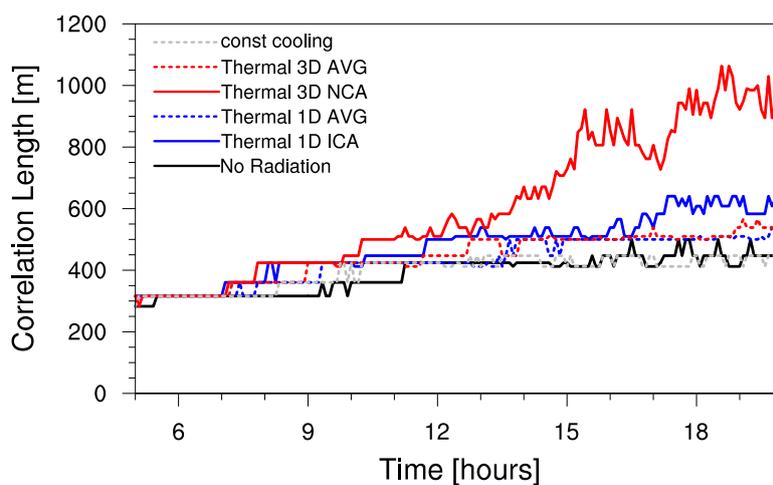
Figure 18. Temporal development of the correlation length for the 100 m resolution simulation. The correlation length is defined by the shift where the correlation coefficient drops below 1/e.
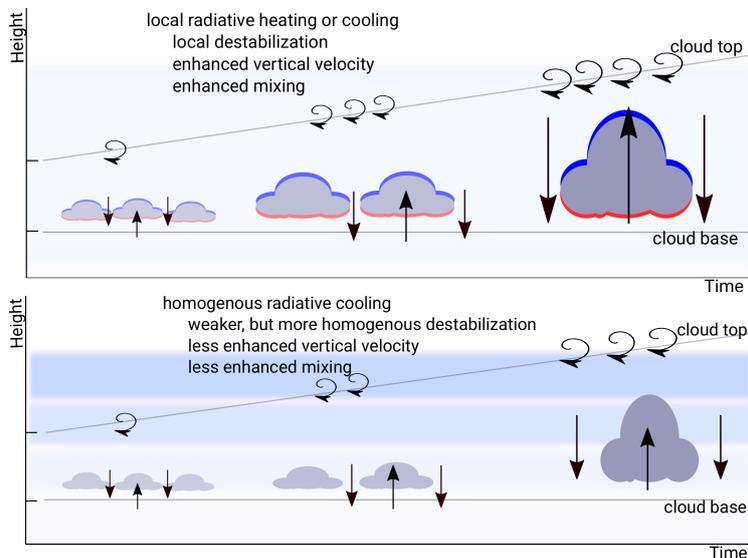
Figure 19. Schematic figure of the effects of thermal radiation in the presented simulations. The figure summarizes cloud development over time and height, showing the enhanced cloud growth, the development of vertical velocity (arrows), a deepening of the cloud layer and the enhanced mixing. Blue and red colors show thermal heating and cooling, either at the clouds itself (for *interactive radiation*) or *averaged* in the cloud layer.